# Supplementary Materials for

## MAVS-dependent Host Species Range and Pathogenicity of Human Hepatitis A Virus

Asuka Hirai-Yuki, Lucinda Hensley, David R. McGivern, Olga Gonzàlez-Lòpez, Anshuman Das, Hui Feng, Lu Sun, Justin E. Wilson, Fengyu Hu, Zongdi Feng, William Lovell, Ichiro Misumi, Jenny P-Y Ting, Stephanie Montgomery, John Cullen, Jason K. Whitmire, Stanley M. Lemon

Correspondence to: smlemon@med.unc.edu

**This PDF file includes:**

## Materials and Methods

### Mice

Mice were bred and housed at the University of North Carolina at Chapel Hill in accordance with the policies and guidelines of the Institutional Animal Care and Use Committee. C57BL/6 mice were purchased from the Jackson Laboratory. *Ifnar1*$^{-/-}$ mice (*36*) backcrossed to C57BL/6 for more than 10 generations were provided by J. Sprent of the Scripps Research Institute. *Ifngr1*$^{-/-}$ mice (*37*), also backcrossed to C57BL/6 for more than 10 generations, were purchased from The Jackson Laboratory. *Ifnar1*$^{-/-}$*Ifngr1*$^{-/-}$ (DKO) mice were a cross between the *Ifnar1*$^{-/-}$ and *Ifngr1*$^{-/-}$ mice and provided by J.L. Whitton of the Scripps Research Institute (*38*). *Mavs*$^{-/-}$ (*Sti*$^{-/-}$) mice (*39*) were provided by M. Gale Jr. of the University of Washington; *Trif*$^{-/-}$ (*Trif*$^{lps2}$) mice (*40*) were originally from the Jackson Laboratory and provided by R. Baric of the University of North Carolina at Chapel Hill. *Irf3*$^{-/-}$ (*Irf3*$^{-/-}$*Bcl2l12*$^{-/-}$) (*41, 42*) and *Irf7*$^{-/-}$ (*43*) mice were provided by T. Taniguchi of the University of Tokyo, and obtained directly from M. Diamond, Washington University. *Irf3*$^{-/-}$*Irf7*$^{-/-}$ (*Irf3*$^{-/-}$*Irf7*$^{-/-}$*Bcl2l12*$^{-/-}$) mice were a cross between *Irf3*$^{-/-}$ and *Irf7*$^{-/-}$ mice (*44*) and also obtained from M. Diamond. *Rag1*$^{-/-}$ mice were originally from the Jackson Laboratory and kindly provided by M. Su of the University of North Carolina at Chapel Hill. NSG mice were purchased from the Jackson Laboratory. All mice except for NSG were on a C57BL/6 background.

### HAV infectious challenge

Mice were intravenously inoculated with the indicated virus inocula at 6-10 weeks of age. Mice were housed in individual cages for collection of fecal pellets with periodic collection of serum samples. Tissues were harvested at necropsy and stored in RNAlater (Thermo Fisher Scientific, Maltham, MA), snap frozen on dry ice and kept at -80 °C, or fixed in 10% neutral phosphate-buffered formalin for 48 hrs and stored in 70% ethanol until processed for histology. All experiments involving mice were approved by the Institutional Animal Care and Use Committee of the University of North Carolina at Chapel Hill.

### Hepatitis A virus (HAV)

All experiments were with the HM175 strain of human HAV (*45*). For the first mouse passage of HAV, DKO mice were inoculated i.v. with an extract of feces from an experimentally-infected chimpanzee (4x0293) (*4*). For successive passages, mice were inoculated i.v. with extracts of fecal pellets from infected mice (collected at the peak of virus shedding) or homogenates of infected liver. Briefly, fecal pellets were homogenized in phosphate-buffered saline (PBS) and clarified by centrifugation at 10,000 x g for 5 min. The supernatant fluid was mixed with an equal volume of chloroform, shaken for 5 min, then centrifuged at 18,000 x g for 5 min. The aqueous phase was removed, placed in a polystyrene cell culture flask at room temperature for 5 min, and aliquots stored at -80 °C. Liver was homogenized in PBS followed by centrifugation at 10,000 x g for 5 min. Supernatant fluids were stored in aliquots at -80 °C. The abundance of HAV RNA (genome equivalent, GE) in fecal and liver inocula was quantified by real-time RT-qPCR. Except where otherwise indicated (mouse passages 1-5), mice were inoculated i.v. with 4$^{th}$ or 5$^{th}$ passage liver extracts from infected DKO or *Mavs*$^{-/-}$ mice containing ~$10^{8.4}$ GE HAV RNA.

Alanine aminotransferase

Serum alanine aminotransferase (ALT) activity was measured using the MaxDiscovery ALT Color Endpoint Assay (Bioo Scientific, Austin, TX).

Quantitative RT-qPCR

RNA was extracted from serum and fecal samples using the QIaAmp Viral RNA Isolation Kit (Qiagen, Valencia, CA). RNA was isolated from tissues using TRIzol reagent (Invitrogen Life Technologies, Carlsbad, CA) according to the manufacturer's suggested protocol. RNA concentration was measured using a NanoDrop (Thermo Scientific, Wilmington, DE). HAV RNA abundance was quantified by RT-qPCR using iScript One Step RT-qPCR Kit for Probes and the iTaq Universal Probes One-Step Kit (Bio-Rad, Hercules, CA) with a CFX96 Real-Time PCR Detection System (Bio-Rad). HAV RNA levels were determined by reference to a standard curve generated with synthetic HAV RNA. Primers targeted sequences in the 5' untranslated RNA segment of the genome: 5'- GGTAGGCTACGGGTGAAAC-3'and 5'-AACAACTCACCAATA TCCGC-3' (*4*). The FAM/TAMRA probe was 5'-CTTAGGCTAATACTTCTATGA AGAGATGC-3'. For quantitation of ISG, cytokine and inflammasome component mRNAs, DNA contamination in tissue RNA extracts was removed using RNase-Free DNase Set (Qiagen). cDNA synthesis was carried out with SurperScript III First-strand Synthesis SuperMix for RT-qPCR Kit (Invitrogen). Probe sets were from TaqMan Gene Expression Assays (Thermo Fisher Scientific); *Isg20* (Mm00469585_m1); *Isg15* (Mm01705338_s1); *Ifit1 (Isg56)* (Mm00515153_m1); *Ifit2 (Isg54)* (Mm00492608_m1); *Cxcl0 (IP10)* (Mm00445235_m1); *Ifnb1* (Mm00439546_s1); *Ifng* (Mm00801778_m1); *Tnf (TNFα)* (Mm00443258_m1); *Il-2* (Mm00439860_m1); *Il-21* (Mm00517640_m1); *Ccl5 (RANTES)* (Mm01302427_m1); *Mip1-α* (Mm00441258_m1); *Pmaip1 (Noxa)* (Mm00451763_m1); and, *Actb* (*β-actin)* (Mm00607939_s1). Amplifications were carried out with TaqMan Universal PCR Master Mix. qPCR assay for *Il1β*, *Nlrp3*, *Caspase1* and *Pycard* were carried out with the SYBR green iTaq Universal SYBR Green Supermix (Bio-Rad). Primers were provided by H. Wen (University of North Carolina at Chapel Hill) (*46*).

Histopathology and *in situ* hybridization (ISH)

Formalin-fixed paraffin-embedded (FFPE) livers were sectioned at 4 μm thickness for histopathology, *in situ* hybridization and immunohistochemistry. Sections were stained with hematoxylin and eosin (H&E) and examined for histological changes by light microscopy. *In situ* hybridization for detection of HAV RNA was carried out using the QuantiGene ViewRNA FFPE Assay (Affymetrix, Santa Clara, CA). The HAV probe set was designed to target the VP1/VP3 region of HM175/p16 (GenBank Accession KP879217.1). Additional probe sets targeted murine Ccl5 (NM_013653, VB6-14424) and albumin (NM_009654, VB6-12839) (Affymetrix). Slides were processed following the QuantiGene protocol. Images were acquired using a Leica SP2 laser-scanning spectral confocal microscope (Leica Microsystems, Buffalo Grove, IL). The percentage of cells infected with HAV was quantified from recorded confocal microscopy images using MetaMorph software (Molecular Devices, Sunnyvale, CA). Cell boundaries were estimated by drawing watershed lines between nuclei. Infected cells were defined as those containing signal above a background threshold that was set based upon images of liver tissue from HAV-naïve mice that were hybridized with the HAV-specific probe set. For dual detection of HAV RNA and cleaved caspase 3, sections were blocked in 10%

goat serum in PBS for 1 hr after completion of *in situ* hybridization, then incubated with antibody to cleaved caspase 3 (9661S, Cell Signaling, Danvers, MA) at a dilution of 1:100 with 1% bovine serum albumin (BSA) in PBS for 2 hrs at room temperature. Anti-rabbit IgG-488 (Life Technologies, Carlsbad, CA) in 1% BSA-PBS was applied at a dilution of 1:300 for 1 hr at room temperature. Images were acquired using a Nikon Eclipse-Ti inverted microscope (Nikon Instruments Inc, Melville, NY).

Immunohistochemistry

Cleaved caspase 3 staining was accomplished using Dako Autostainer (Dako, Carpinteria, CA). Tissue sections were de-paraffinized and rehydrated prior to antigen retrieval in a Pascal presser cooker (Dako) for 30 sec at 123 °C with 18 lbs pressure in Tris-EDTA buffer (10 mM Tris base, 1 mM EDTA, 0.05% Tween 20, pH 9.0). Slides were cooled and rinsed with PBS, then treated sequentially with endogenous peroxidase blocker and universal block prior to incubation for 2 hr at room temperature with antibody to cleaved caspase 3 (9661S, Cell Signaling) diluted 1:100, and 30 min at room temperature with ImmPress HRP Rabbit IgG Polymer (Vector, Burlingame, CA). Slides were developed with DAB (3,3'-diaminobenzidine), counterstained with Meyer's hematoxylin, dehydrated, and mounted in mounting media. Two-color immunohistochemistry for detection of CD8 and CD4 was carried out by the Animal Histopathology Core Facility of the Lineberger Comprehensive Cancer Center of the University of North Carolina at Chapel Hill using a Discovery Ultra Automated IHC staining system (Ventana, Tucson, USA). Tissue sections were de-paraffinized and rehydrated prior to antigen retrieval using Cell Conditioning 1 Solution (CC1) (Ventana) for 64 min at 90°C and incubation with a protein block for 1 hr at room temperature. The slides were given a hydrogen peroxide block for 8 min at room temperature and then incubated in anti-mouse CD8a (14-0808, 1:100, eBioscience, San Diego, CA) diluted in Discovery PSS Diluent (Ventana) at 1:100 for 1h at room temperature, followed by OmniMap anti-rat IgG-HRP (760-4457, Ventana) for 32 min at room temperature. The slides were treated with DAB and subjected to antibody denaturation at 95°C for 8 minutes to prepare for CD4 staining. Additional antigen retrieval was carried out using CC1 for 24 minutes at 100°C followed by a protein block for 1 h at room temperature. The slides were given a hydrogen peroxide block for 8 min at room temperature followed by incubation with anti-mouse CD4 antibody (14-9766, eBioscience) diluted in Discovery Ab Diluent (Ventana) at 1:20 for 4 hrs at room temperature, and anti-rat IgG-HRP (Dako) at a 1:100 dilution for 1 hr at room temperature. The slides were treated with Discovery Purple (Ventana) for 100 min, and counterstained with Hematoxylin II for 12 min and then Bluing Reagent (Ventana) for 4 min.

Terminal deoxynucleotidyl transferase dUTP nick-labeling (TUNEL)

FFPE liver sections were de-paraffinzed, rehydrated and incubated with protease QF solution provided with the Affymetrix QuantiGene ViewRNA FFPE Assay at 37 °C for 20 min. Terminal deoxynucleotidyl transferase mediated dUTP nick end labeling (TUNEL) was carried out using the *In situ* Cell Death Detection Kit (Roche, Basel, Schweiz). Images were acquired using a Nikon Eclipse-Ti inverted microscope (Nikon Instruments, Inc).

Anti-HAV IgG ELISA

Serum anti-HAV IgG was quantified with a modification of a previously described HAV capsid antigen ELISA (*8*). HM175/18f HAV (*47*) produced in cell culture was inactivated by UV irradiation and captured by human convalescent antibody (JC plasma) coated on a 96-well polystyrene plate. Three-fold serial dilutions of mouse serum samples starting at a 1:33 dilution were incubated in the wells of the plate at room temperature for 1 hr, followed by incubation with horseradish peroxidase-conjugated goat-anti-mouse antibody (Southern Biotech, Birmingham, AL) at room temperature for 1 h. Following the addition of substrate (3,3',5,5'-tetramethylbenzidine), $OD_{450}$ was determined using a Synergy 2 (BioTek, Winooski, VT) microplate reader. Anti-HAV capsid monoclonal antibody K24F2 (Commonwealth Serum Laboratories, Victoria, Australia) was included in assays as a positive control.

Neutralizing antibody assay

Cell culture-derived HM175/18f virus (*47*) ($7.2 \times 10^4$ GE/50 µl) was mixed with an equal volume of heat-inactivated serum diluted in PBS at 1:10 or more, then incubated at 37 °C for 1 hr. Human convalescent antibody (JC plasma) and anti-HAV monoclonal antibody K24F2 (Commonwealth Serum Laboratories, Victoria, Australia) were included as positive controls. The virus-serum mixture was inoculated onto Huh-7.5 or FRhK-4 cell monolayers in 12-well plates and allowed to adsorb for 2 hrs at 36 °C prior to the addition of medium containing 1% methyl cellulose and 2% FBS. Following 8-11 days incubation at 36 °C in a 5% $CO_2$ atmosphere, cells were fixed with 4% PFA then processed subsequently for infrared fluorescent immunofocus assay (IR-FIFA) (*48*). The cell sheet was permeabilized with 0.25% Triton X-100, blocked with 10% normal goat serum in PBS, and incubated with K24F2 diluted 1:600 in 3% BSA in PBS overnight at 4 °C. The cells were washed with PBS and incubated for 1 hr at room temperature with IRDye 680LT anti-mouse (1 µg/ml, LI-COR Bioscience, Lincoln, NE) in 3% BSA-PBS prior to visualization of replication foci by scanning with an Odyssey infrared imaging system (LI-COR Bioscience).

Immunoblots

Frozen mouse liver samples were homogenized in the presence of lysis buffer (20% w/v, Tissue Extraction Reagent, Invitrogen) containing protease inhibitors (Sigma-Aldrich), 1 mM $Na_3VO_4$, and 50 mM NaF, clarified by centrifugation twice at 16,000 x g for 30 min at 4 °C, and stored at -80 °C. The samples were subjected to SDS-PAGE and immunoblotting using standard methods. Blots were blocked with Odyssey blocking buffer (LI-COR Bioscience) and probed with the following primary antibodies: IRF3 (sc-9082 1:200, Santa Cruz Biotech, Dallas, TX), pIRF3 (4947 1:200, Cell Signaling), ISG15 (sc-50366 1:200, Santa Cruz Biotech), Bax (2772S 1:1000, Cell Signaling), NF-κB p65 (8242S 1:1000, Cell Signaling) and phospho-p65 (3033S 1:1000, Cell Signaling), cleaved caspase 3 (9661S 1:1000, Cell Signaling), cleaved caspase 8 (9429S 1:1000, Cell Signaling), cleaved caspase 9 (9509S 1:1000, Cell Signaling) and β-actin (AC-74 1:10000, Sigma). Infrared conjugated secondary antibodies (LI-COR Bioscience) were used to visualize protein bands with an Odyssey infrared imaging system (LI-COR Bioscience). Extracts of AML12 cells, a mouse hepatocyte cell line (ATCC CRL2254), treated with 4 µg/ml actinomycin D (Sigma-Aldrich, St. Louis, MO) and 100 ng/ml recombinant mouse TNF-α (Sigma-Aldrich) or DMSO for 6 h, served as controls for

caspase immunoblots. AML12 cells were treated with 100 ng/ml of TNF-α for 30 min for use as a control for p65 immunoblots.

Caspase activity

Caspase 3/7, 8 and 9 activities were measured in liver tissue extracts using the Caspase-Glo 3/7, 8 and 9 kits (Promega, Madison, WI) (*49*). Frozen liver was homogenized in a hypotonic extraction buffer (25mM HEPES, pH7.5, 5 mM $MgCl_2$ and 1 mM EGTA) containing protease inhibitors (Sigma-Aldrich), and centrifuged at 16,000 x g for 30 min at 4 °C and stored at -80 °C. Equal volumes of reagents and 10 μg/ml cytosolic protein was added to a white-walled 96-well plate and incubated at room temperature for 1 h. Luminescence was measured using a Synergy 2 microplate reader (BioTek) (*50*).

Cytokine assay

Serum cytokines were quantified using Verkine-HS Mouse IFN-β ELISA (PBL Assay Science, Piscataway, NJ), and IFN-γ, TNF-α, IL-6 and IL-1β Platinum ELISA (eBioscience) assays: limits of detection were IFN-γ (26.5 pg/ml), TNF-α (7.4 pg/ml), IL-6 (15 pg/ml) and IL-1β (7.8 pg/ml). Cytokine levels were quantified in liver homogenates prepared as described above for immunoblotting using a Luminex Bead-based Multiplex Assay targeting IFN-γ, TNF-α, IL-1β, IL-2, IL-4, IL-5, IL-6, CCL3, CCL4, CCL5 (RANTES), CXCL9, and CXCL10 (R&D Systems, Minneapolis, MN).

Enumeration of intrahepatic immune cells

Following removal of the left lobe of the liver for RNA assays, the remaining liver was perfused *in situ* with 10 ml PBS. The excised and disrupted liver was then digested in RPMI 1640 media containing 1mM $CaCl_2$, 1mM $MgCl_2$ and 100 U/ml type IV collagenase (Gibco/Thermo scientific, Waltham, MA) at 37 °C for 30 min, and cells were passed through a 100-μm cell strainer. After centrifugation at 500 x g for 10 min at 4 °C, cells were washed twice with cold RPMI containing 1% FBS, then resuspended in 37.5% Percoll (GE Healthcare Life Sciences, Pittsburgh, PA) and re-centrifuged at 500 x g for 15 min at room temperature. After hemolysis in ACK (ammonium-chloride-potassium) buffer, cells were washed with FACS buffer (PBS, 1% BSA and 0.2% $NaN_3$) and stained with antibodies against NK1.1 (PK136), CD3 (17A2), CD4 (RM4-5), CD8 (53-6.7), TCR γ/δ (GL3), CD11b (M1/70) and F480 (BM8) (all from BioLegend, San Diego, CA). Cell staining was analyzed by four-color flow cytometry using a FACSCalibur (BD Biosciences, San Jose, CA) and analyzed using FlowJo software (FLOWJO, Ashland, OR).

*Ex vivo* peptide stimulation of T cells

Splenic lymphocytes were isolated from HAV-infected mice and stimulated with 5 peptide pools comprising in aggregate 222 peptides, each 20 amino acids in length and spanning the entire wild-type HM175 virus polyprotein sequence with 10 amino acid overlap (*51*). Cells were isolated and resuspended in media (RPMI and 10% FBS), followed by the addition of GolgiPlug (BD Biosciences, San Jose, CA), then incubated in the presence or absence of 1 μg/ml peptide pools at 37 °C for 5 hr. At the end of incubation, cells were washed with FACS buffer and stained with antibodies recognizing cell surface markers. Cells were then washed with FACS buffer, fixed (Fixation buffer, BioLegend), permeabilized using Permeabilization/Wash buffer (BioLegend) and stained

for intracellular IFNγ (BioLegend, XMG1.2) prior to analysis on a FACSCalibur (BD Biosciences) cytometer and FlowJo software (FLOWJO).

NK/NKT, $CD4^+$ and $CD8^+$ T cell depletion

Depletion of NK/NKT cells in *Ifnar1*$^{-/-}$ mice was accomplished by intraperitoneal administration of 3 doses of 75 μg NK1.1-PK136 antibody (BioXCell, West Lebanon, NH) 3 and 2 days prior to, and then again 7 days after i.v. virus challenge. Control mice were administrated three doses of 75 μg rat IgG2a isotype control on the same schedule. To deplete $CD4^+$ or $CD8^+$ T cells, mice were administrated two doses of 250 μg GK1.5 (anti-CD4) (BioXCell) or/and Lyt2-2.43 (anti-CD8) (BioXCell) antibody 3 and 1 days prior to i.v. inoculation of virus. Control mice were given two doses of 250μg rat IgG2b isotype control antibody on the same schedule. To confirm cell type-specific depletion, spleen cells were isolated and stained for cell markers as described above.

Macrophage depletion

*Ifnar1*$^{-/-}$ mice were depleted of macrophages by intravenous injection of 200 μl clodronate liposomes (ClodLip BV, Amsterdam) 1 day prior to and again 3 days following HAV challenge. Control animals were similarly inoculated with an equal volume of PBS liposomes. To confirm macrophage depletion, cells were isolated from the liver and spleen of similarly treated wild-type C57BL/6 mice and stained for macrophage markers F4/80 and CD11b.

In vitro MAVS cleavage assay

Embryonic fibroblasts (MEFs) from *Mavs*$^{-/-}$ mice were provided by M. Gale, Jr of the University of Washington. The MAVS coding sequence from pcDNA3.1-muMAVS-V5 (*13*) was cloned into *Hind*III-*Bam*HI linearized pEGFP-C1 (Clontech, Mountain View, CA). Expression vectors for GFP-tagged human MAVS, HAV 3ABC protease, with or without a C172A active-site substitution as well as the corresponding empty construct-pCMV-HA have been described previously (*13,52*). Transfections were carried out with Fugene HD (Promega, Madison, WI) according to the manufacturer's protocol. Cells were lysed 48 hr post-transfection for immunoblotting as described (*13*). Primary antibodies were polyclonal anti-rodent MAVS (4983 1:1000, Cell Signaling), polyclonal anti-human MAVS (AT107 1:2000, Enzo Life Sciences, Farmingdale, NY), monoclonal anti-HA (3724 1:5000, Cell Signaling) and anti-β-actin (AC-74 1:1000, Sigma). Infrared conjugated secondary antibodies (LI-COR Bioscience) were used for development. Protein bands were visualized with an Odyssey infrared imaging system (LI-COR Bioscience).

HAV nucleotide sequence

RNA isolated from murine feces or liver as described above was reverse-transcribed into cDNA using the SurperScript III First-Strand Synthesis System for RT-qPCR kit and random primers (Invitrogen). Overlapping cDNA segments were amplified using primer sets that span the HAV genome and subjected to automated DNA sequencing using standard methods. Sequences were deposited in GenBank with the accession numbers: KX343014, KX343015, KX343016, KX343017, and KX343018.

Isopycnic gradient ultracentrifugation

Liver homogenate was clarified by centrifugation at 10,000 x g for 30 min at 4°, then loaded onto a preformed 8-40% iodixanol (Opti-prep, Sigma Aldrich) step gradient

in a 5 ml ultracentrifuge tube (Beckman Coulter, Indianapolis, IN) (*8*). After centrifugation at 37,000 rpm in a Beckman SW55i rotor for 24 hr at 4°C in a Beckman Optina LE-80K ultracentrifuge, 20 fractions were collected from the top of the gradient and the HAV RNA content of each determined by RT-qPCR. The density of gradient fractions was determined by refractometry.

Statistical analysis

Statistical tests were carried out using Prism 6 for Mac OS X software (GraphPad Software, La Jolla, CA). Unless otherwise noted, comparisons between groups used the non-parametric Mann-Whitney test, or one-way or two-way ANOVA.

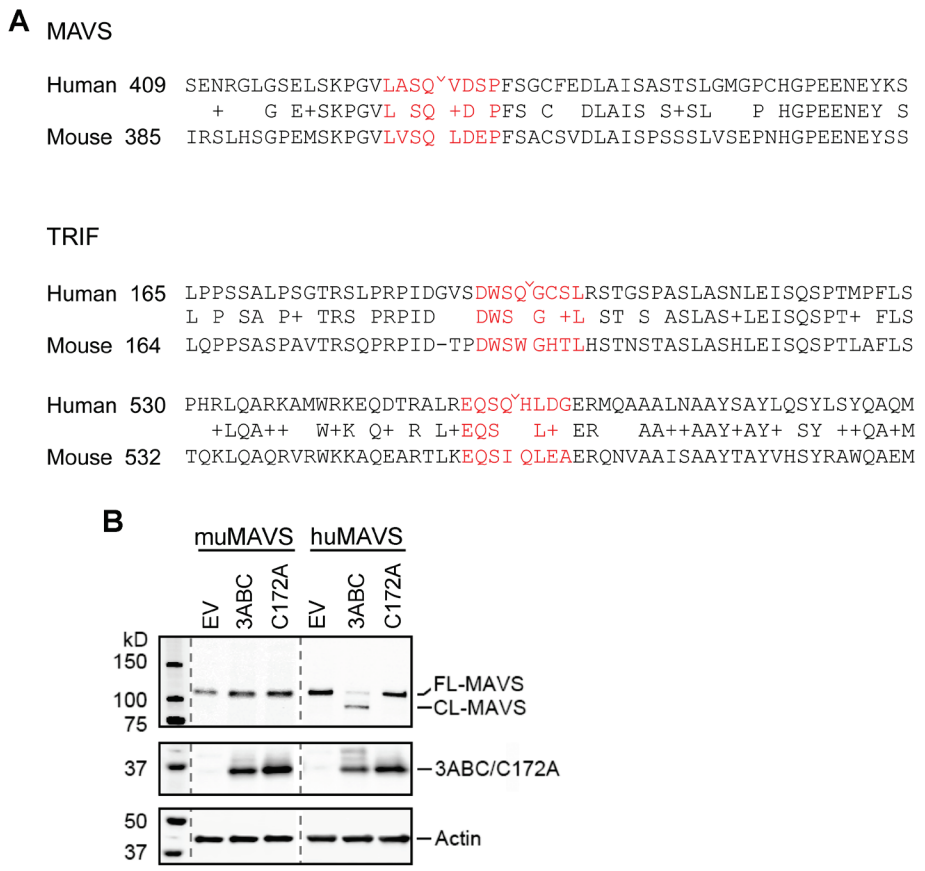


**Fig. S1. Murine MAVS and TRIF orthologs as potential targets of HAV-encoded proteases.** (**A**) Partial alignments of human (top) MAVS and (bottom) TRIF protein sequences with their murine orthologs. Arrowheads denote sites at which the HAV 3ABC proteinase cleaves human MAVS and HAV 3CD proteinase cleaves human TRIF (TICAM-1) (*13,14*). (**B**) *In vivo* MAVS cleavage assays. Murine *Mavs*$^{-/-}$ embryonic fibroblasts were co-transfected with vectors expressing GFP-tagged murine or human MAVS (muMAVS and huMAVS, respectively) and HA-tagged HAV 3ABC proteinase, with or without a C172A active-site substitution that eliminates its catalytic activity. Cells were lysed and extracts subjected to immunoblotting with antibodies to huMAVS and muMAVS and the HA tag. MAVS cleavage (CL-MAVS) occurred only in cells expressing human MAVS and catalytically active 3ABC. All samples were run on the same gel; EV= empty vector; β-actin was included as a loading control.

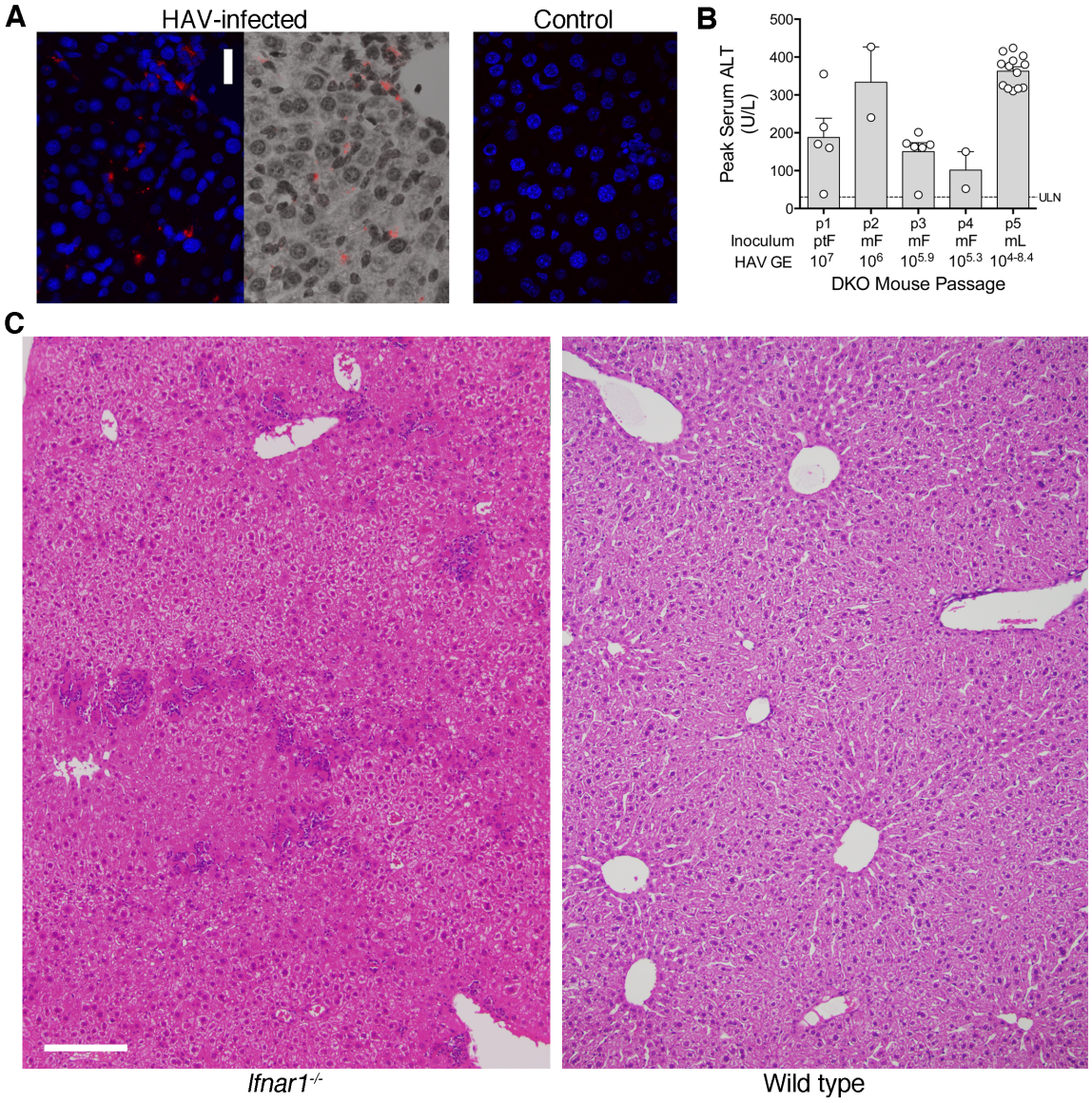


**Fig. S2. Serial passage of HAV in *Ifnar1*$^{-/-}$*Ifngr1*$^{-/-}$ (DKO) and *Ifnar1*$^{-/-}$ mice.**
(**A**) HAV RNA detected by *in situ* hybridization (ISH): (left) fluorescence and bright field images of infected DKO liver 37 d.p.i.; (right) control DKO mouse (bar = 25 μm). (**B**) Peak serum ALT during serial passage of virus. Note that passage 4 was terminated at 18 d.p.i (see Fig. 1C). 'ptF', chimpanzee fecal virus; 'mF' mouse fecal virus; 'mL', mouse liver virus; 'ULN', upper limits normal. (**C**) H&E stained sections of liver from (left) an HAV-infected *Ifnar1*$^{-/-}$ mouse 161 d.p.i (ALT = 101 IU/L) showing multiple inflammatory foci with apoptotic or necrotic hepatocytes vs. (right) a wild-type Bl6 mouse that received the same 4$^{th}$ passage DKO liver inoculum with normal liver architecture and no inflammatory foci. Bar = 100 mμ.

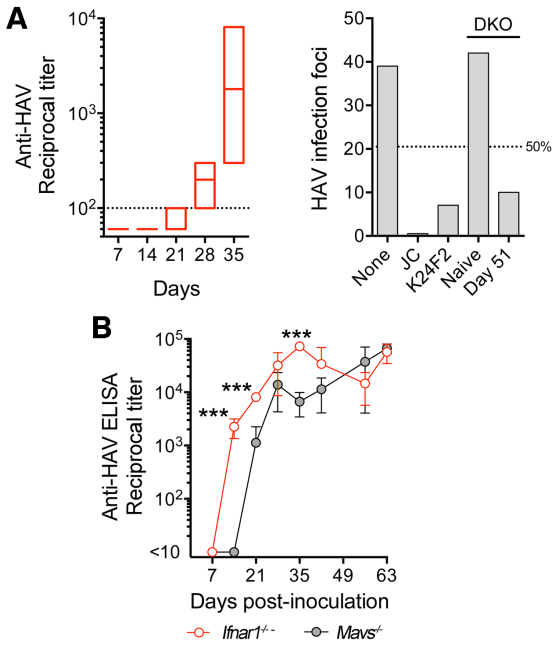


**Fig. S3. Antibody responses to HAV in infected DKO, *Ifnar1*$^{-/-}$ and *Mavs*$^{-/-}$ mice.** (**A**) (left) Anti-HAV response in DKO mice (3rd passage); floating bars represent maximum, median, and minimum ELISA titer. n=6. (right) Serum neutralizing antibody activity pre- and 51 days post-infection in a DKO mouse (JC, human polyclonal anti-HAV; K24F2, murine monoclonal anti-HAV antibody). Similar results were obtained with serum from *Ifnar1*$^{-/-}$ mice. (**B**) Anti-HAV measured by ELISA in sera from *Ifnar1*$^{-/-}$ vs. *Mavs*$^{-/-}$ mice. Data are mean ± SD, n=4-5. ***p<0.001 by multiple t-test with false discovery rate 1%.

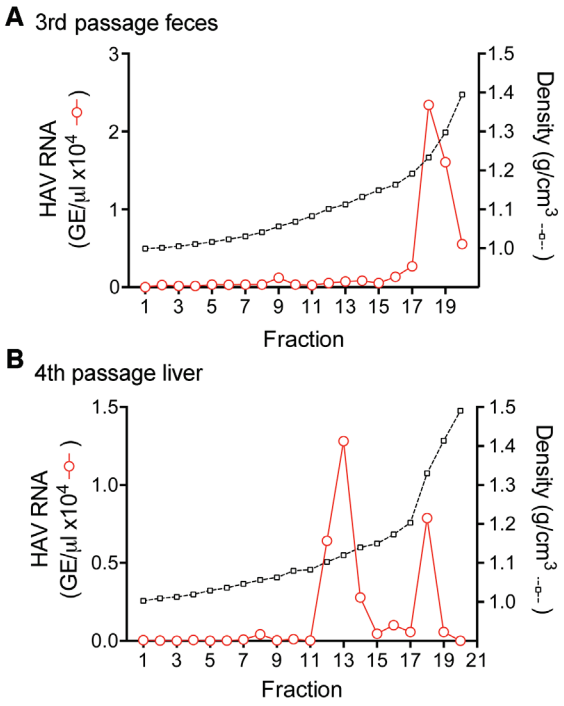


**Fig. S4. Isopycnic density gradient centrifugation of HAV inocula.** Preformed iodixanol step gradients were loaded with inocula derived from (**A**) 3rd passage DKO feces or (**B**) 4th passage DKO liver extract, and centrifuged to equilibrium as described (*8*). Fractions were collected from the top and assayed for HAV RNA by RT-PCR. Peak density of fecal virus was ~1.28 g/cm$^3$ ('naked' particles). Two HAV species were present in the liver extract, banding at ~1.11 g/cm$^3$ (membrane-associated) and 1.30 g/cm$^3$ (naked virions).

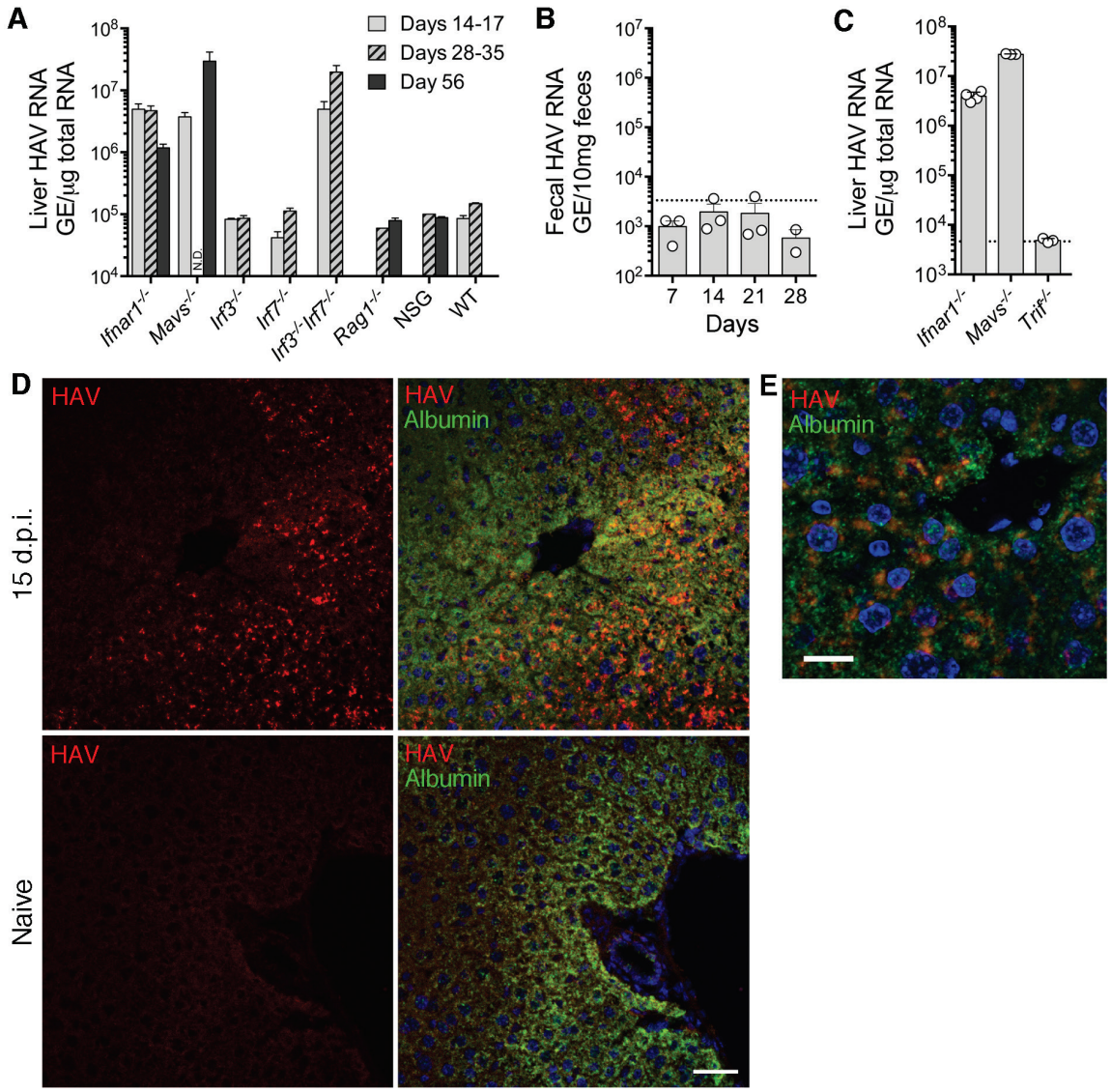


**Fig. S5. Fecal and hepatic HAV RNA following virus challenge of knockout mice.** (**A**) Intrahepatic HAV RNA at intervals after i.v. challenge of *Ifnar1*$^{-/-}$, *Mavs*$^{-/-}$, *Irf3*$^{-/-}$, *Irf7*$^{-/-}$, *Irf3*$^{-/-}$*Irf7*$^{-/-}$, *Rag1*$^{-/-}$, NSG, and WT mice. Data are mean ± range or SEM, n=2-5. (**B**) Fecal (7-28 d.p.i.) and (**C**) hepatic HAV RNA (28 d.p.i.) in *Trif*$^{-/-}$ mice, with liver from infected *Ifnar1*$^{-/-}$ and *Mavs*$^{-/-}$ mice (14-15 d.p.i.) shown for comparison. Data are mean ± SEM, n=3. Horizontal lines indicate mean + 2 SD values from fecal extracts [n=40] or liver tissue [n=10] from HAV-naïve mice. (**D**) Confocal microscopic images showing *in situ* hybridization for HAV RNA (red) and albumin mRNA (green) in liver tissue from (top) an HAV-infected *Mavs*$^{-/-}$ mouse 15 d.p.i and (bottom) a control HAV-naïve *Mavs*$^{-/-}$ mouse. Panels on the left show red channel (HAV RNA) only. Tissues were counterstained with DAPI to visualize nuclei. Bar = 40 µm. (**E**) Higher magnification view of HAV-infected *Mavs*$^{-/-}$ tissue with *in situ* hybridization for HAV RNA (red) and albumin mRNA (green) as in panel D. HAV RNA is present in the cytoplasm of numerous hepatocytes near a central vein. Bar = 20 µm.

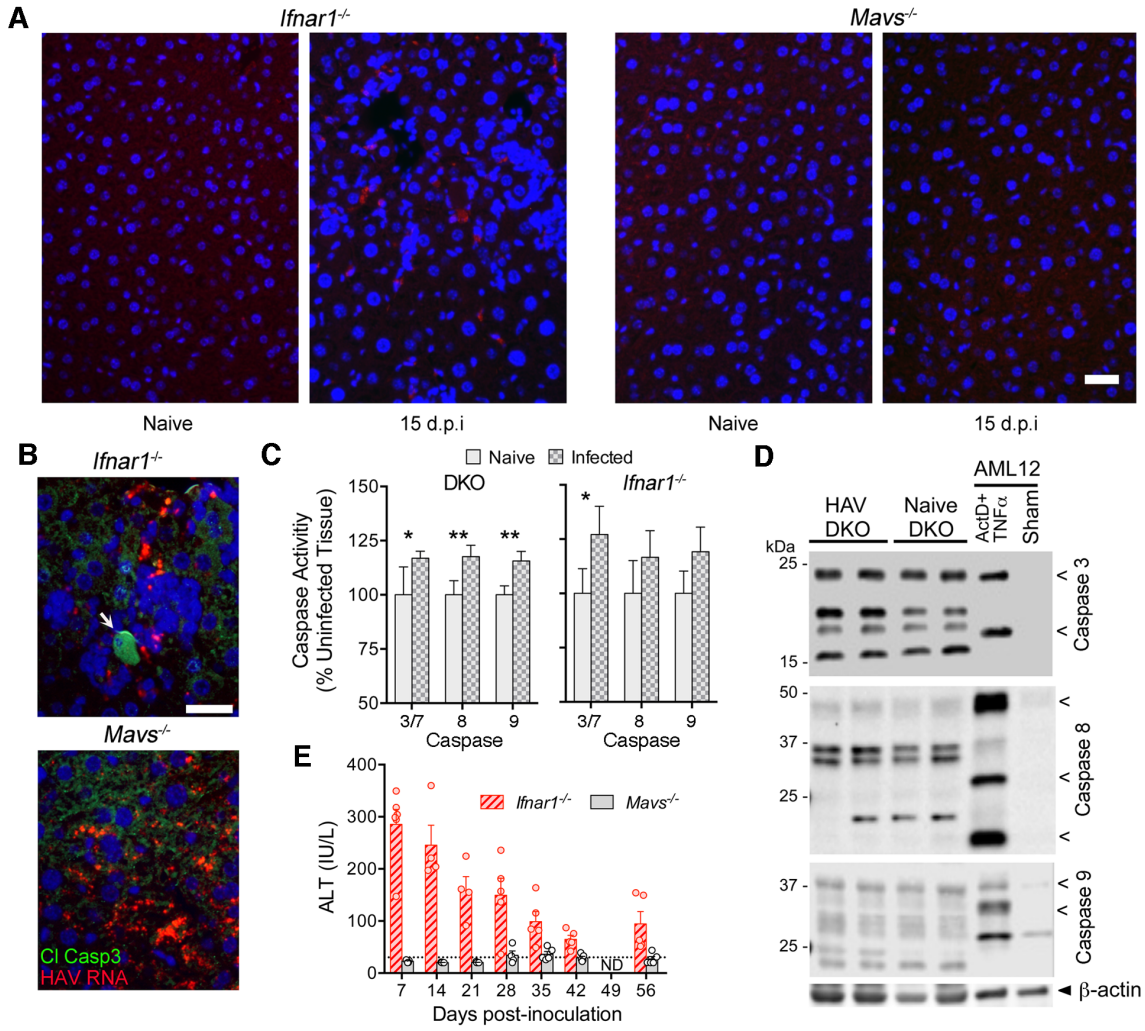


**Fig. S6. Hepatocellular apoptosis in HAV-infected *Ifnar1*$^{-/-}$ mice.** (**A**) TUNEL stain (red) of (left) naïve and infected *Ifnar1*$^{-/-}$ and (right) naïve and infected *Mavs*$^{-/-}$ mouse liver, 15 d.p.i. ALT was 374 IU/ml in the infected *Ifnar1*$^{-/-}$ mouse versus 37 IU/ml in the infected *Mavs*$^{-/-}$ mouse. Bar = 50 µm. (**B**) Dual immunofluorescence assay for cleaved caspase 3 (green) and ISH for HAV RNA (red). The arrow identifies a single cell with cleaved caspase staining surrounded by hepatocytes containing HAV RNA in an *Ifnar1*$^{-/-}$ mouse (top). Infected *Mavs*$^{-/-}$ liver (bottom) contains more HAV RNA, but shows no apoptosis. Bar = 20 µm. (**C**) CaspaseGlo assays (Promega) for caspase 3/7, 8 and 9 activities in liver tissue from HAV-infected and uninfected DKO and *Ifnar1*$^{-/-}$ mice 7 d.p.i. Data are mean ± SD, n=4. *p<0.05, **p<0.01 naïve vs. infected by t test. (**D**) Cleaved caspase 3, 8, and 9 were not detected in immunoblots of extracts of infected DKO mouse liver. Controls are extracts of actinomycin D/TNF-α-treated vs. sham-treated murine AML12 cells. β-actin was a loading control. (**E**) Serum ALT in infected *Ifnar1*$^{-/-}$ and *Mavs*$^{-/-}$ mice over 56 days. Data are mean ± SEM, n=3-5. ND = not determined.

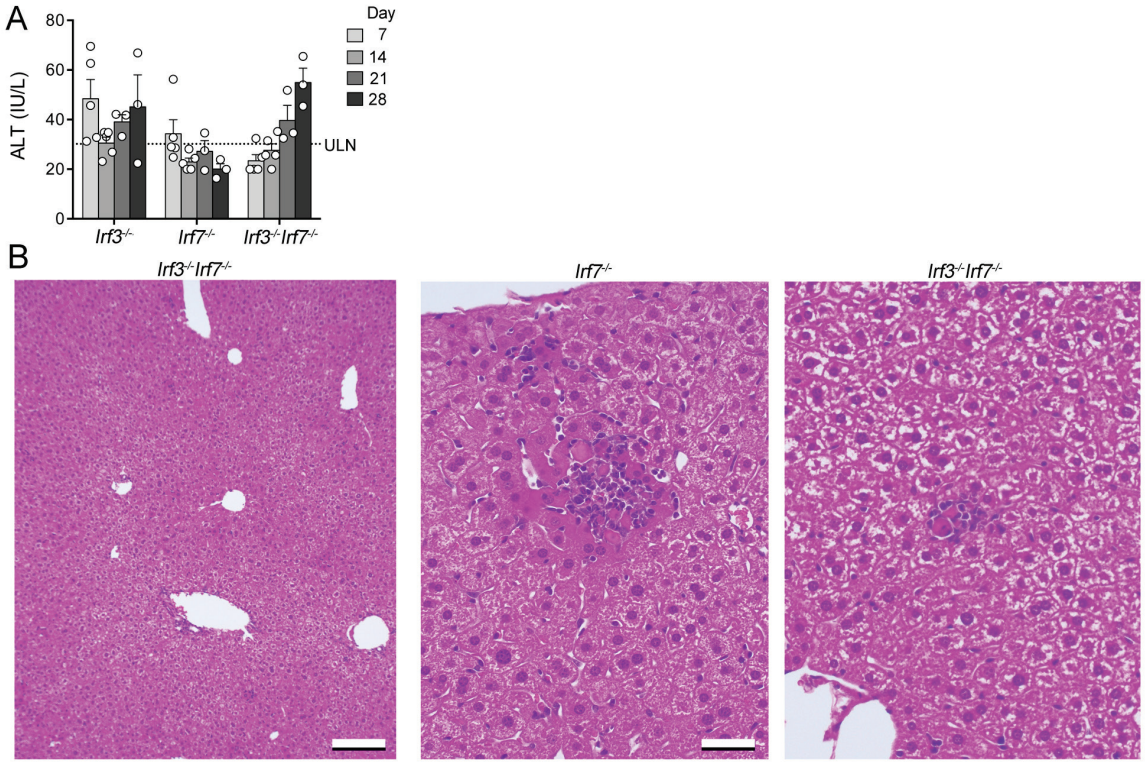


**Fig. S7. HAV infection in *Irf3*$^{-/-}$, *Irf7*$^{-/-}$ and *Irf3*$^{-/-}$*Irf7*$^{-/-}$ double-knockout mice.** (**A**) Serum ALT between 7 and 28 d.p.i. Data are mean ± SEM, n=3-4. 'ULN'=upper limit of normal, (mean + 2 SD in n= 30 naive mice, 30.2 IU/L). (**B**) (left) Low power micrograph of infected *Irf3*$^{-/-}$*Irf7*$^{-/-}$ liver showing an absence of inflammatory foci 17 d.p.i. Bar = 80 µm. (center and right) 40x views of infected (center) *Irf7*$^{-/-}$ and (right) *Irf3*$^{-/-}$*Irf7*$^{-/-}$ liver showing solitary inflammatory lesions with apoptotic cells 17 d.p.i. Bar = 20µm.

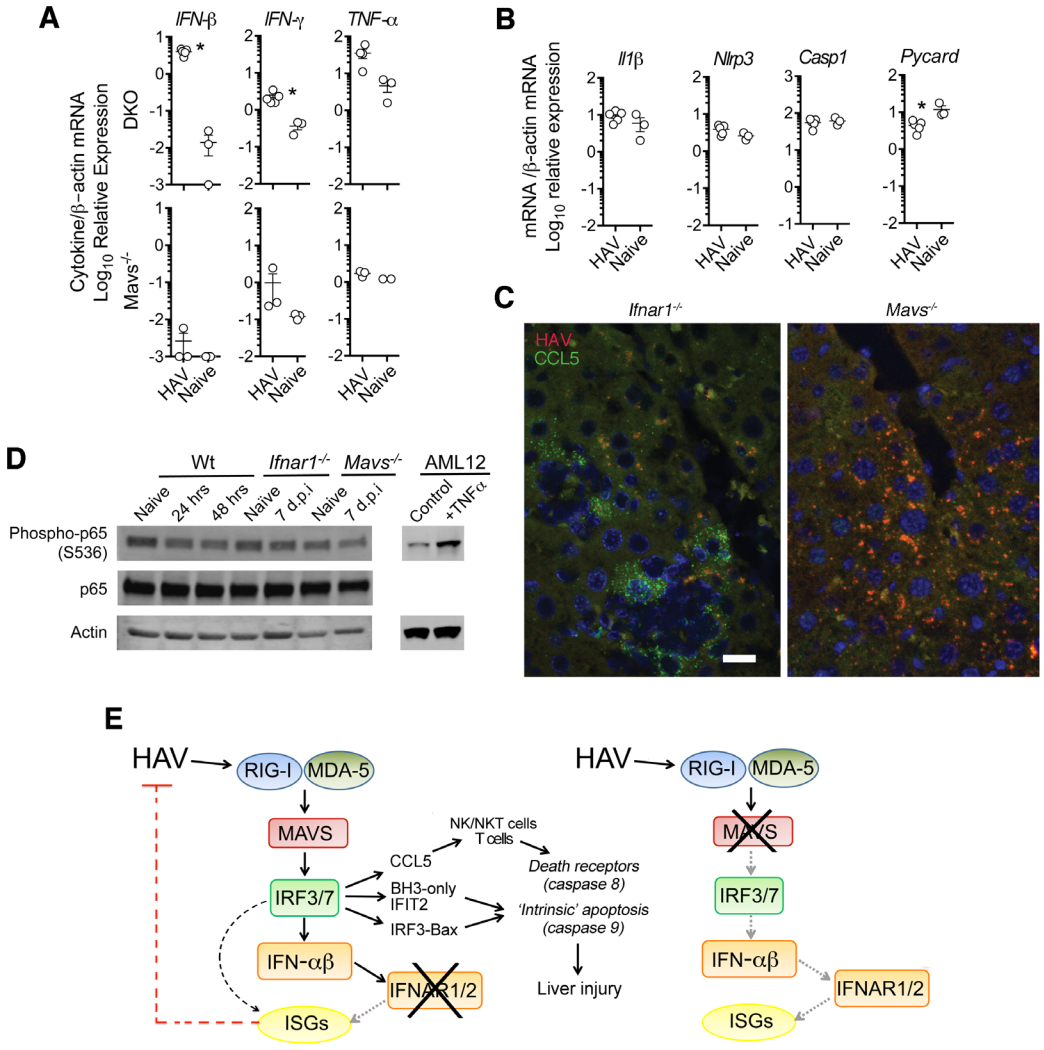


**Fig. S8. Cytokine expression in HAV-infected mice.** (**A**) Relative IFN-β, IFN-γ and TNF-α mRNA expression determined by RT-PCR in liver extracts from infected (top panels) DKO (*Ifnar1*$^{-/-}$*Ifngr1*$^{-/-}$, mean ± SEM, n=5, mean ALT = 243.8 IU/L) and *Mavs*$^{-/-}$ (mean ± SEM, n=3, mean ALT 26.4 IU/L) mice versus HAV-naïve mice (mean ± SEM, n=3). *p<0.05 by two-sided Mann-Whitney test. (**B**) Relative inflammasome-related protein mRNAs in naïve (mean ± SEM, n=3) vs. HAV-infected DKO mice (mean ± SEM, n=5). *p<0.05 by two-sided Mann-Whitney test. (**C**) HAV RNA (red) and CCL5 mRNA (green) visualized by *in situ* hybridization in HAV-infected *Ifnar1*$^{-/-}$ and *Mavs*$^{-/-}$ mice 15 d.p.i. CCL5 expression is prominent in hepatocytes. Nuclei are counterstained with DAPI. Bar = 20 µm. (**D**) Immunoblots of phospho-p65 and total p65 component of NF-κB in livers of infected *Ifnar1*$^{-/-}$ versus *Mavs*$^{-/-}$ mice. Extracts of AML12 cells, treated or not treated with TNF-α, were included as a positive control. (**E**) Innate immune signaling with (left) potential mechanisms of IRF3/7-mediated apoptosis of hepatocytes in HAV-infected *Ifnar1*$^{-/-}$ mice, and (right) virus-induced signaling blocked above IRF3/7 in infected *Mavs*$^{-/-}$ mice.

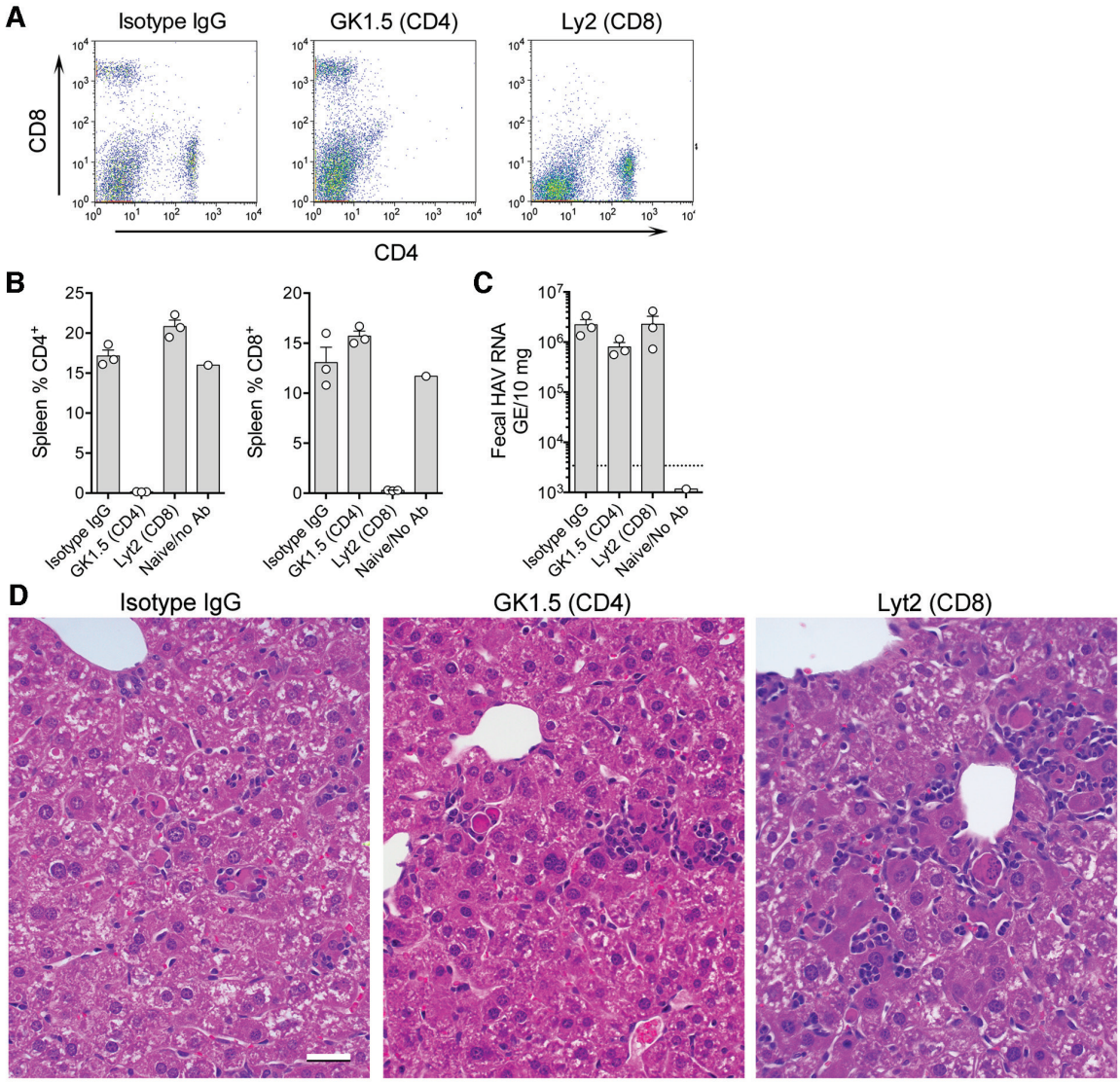


**Fig. S9. Impact of CD4$^+$ or CD8$^+$ T cell depletion on acute HAV-induced liver injury.** *Ifnar1*$^{-/-}$ mice were given 0.25 mg of GK1.5 (CD4), Lyt2/2.43 (CD8), or isotype control antibody i.p. twice, 4 and 1 day prior to i.v. HAV challenge. (**A**) Sample flow cytometry data plots and (**B**) summary of flow cytometry data showing numbers of CD8$^+$ and CD4$^+$ T cells in the spleens of mice 7 d.p.i. (data are mean ± SEM, n=3 in each treatment group) (**C**) Fecal HAV shedding 7 d.p.i. (data are mean ± SEM, n=3). (**D**) H&E stained sections of HAV-infected liver from representative (left) isotype IgG control, (center) anti-CD4, and (right) anti-CD8 antibody-treated mice, demonstrating equivalent degrees of inflammation and hepatocellular apoptosis. Liver tissues from depleted and nondepleted mice indistinguishable when examined blindly. Bar = 20 μm.

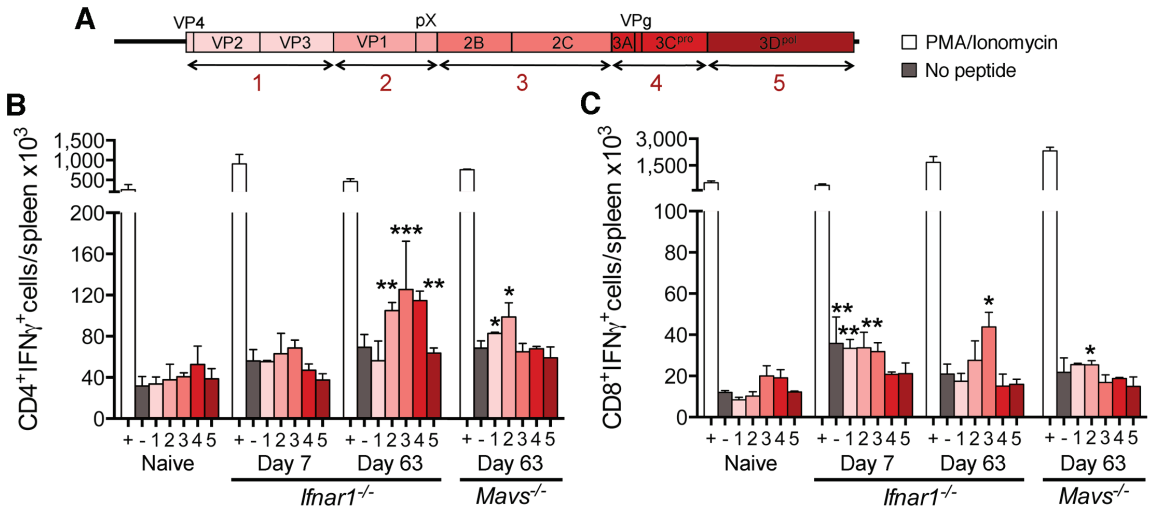


**Fig. S10. Virus-specific CD4$^+$ and CD8$^+$ T cell response in HAV-infected mice.** Cells were harvested from spleens of HAV-infected *Ifnar1*$^{-/-}$ mice (n=3) 7 and (n=2) 63 d.p.i, and *Mavs*$^{-/-}$ mice (n=2) 63 d.p.i. and stimulated *ex vivo* by incubation with (**A**) 5 peptide pools (numbered 1-5), containing in aggregate 222 peptides (each 20 amino acids in length, overlapping by 10 amino acids) spanning the entire wild-type HM175 virus polyprotein sequence (*51*). Controls included: (+) stimulation with phorbol myristic acid (PMA) and ionomycin, and (−) incubation with no peptide. Peptide-stimulated (**B**) CD4$^+$ and (**C**) CD8$^+$ T cells with positive intracellular staining for IFNγ were enumerated by flow cytometry. Data are mean ± SEM, n as above. *p<0.05, **p<0.01, ***p<0.001 versus naïve mice (n=3, 2 *Ifnar1*$^{-/-}$ and 1 *Mavs*$^{-/-}$) by 2-way ANOVA with Dunnett's correction for multiple comparisons.

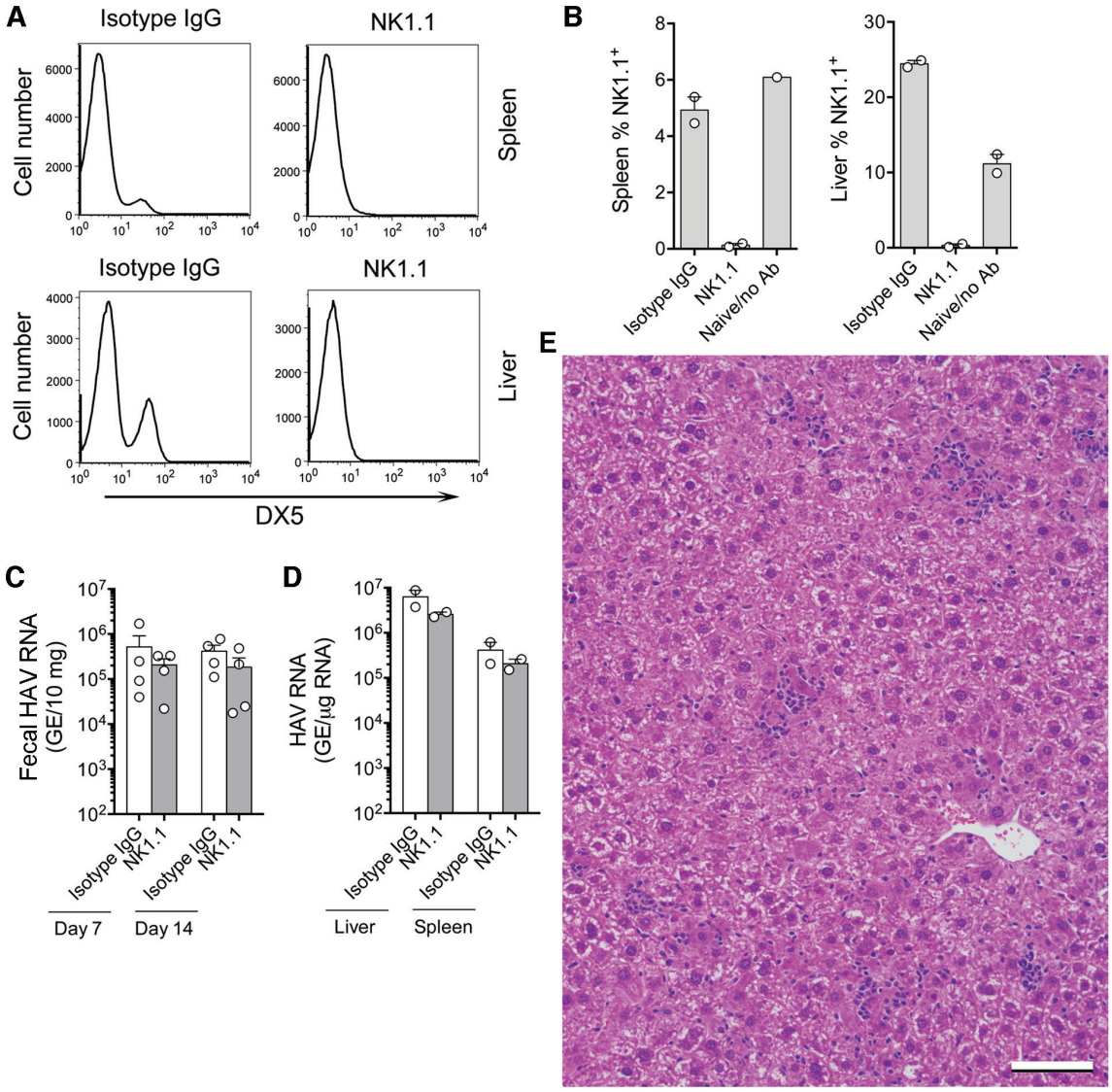


**Fig. S11. Impact of NK cell depletion on HAV-induced acute liver injury**. *Ifnar1*$^{-/-}$ mice received 75μg NK1.1 or isotype control antibody by i.p. injection twice, 3 and 2 days prior to infection, and then again 7 d.p.i. Animals were necropsied 14 d.p.i. (**A**) Sample flow cytometry histograms showing numbers of NK1.1$^{+}$ cells in the spleen (top panels) and liver (bottom) of HAV-infected and uninfected control animals 14 d.p.i. (**B**) Summary of flow cytometry studies. (**C**) Fecal HAV RNA and (**D**) HAV RNA present in liver and spleen of NK cell-depleted vs. control animals. Data are mean ± SEM, n= 4 (feces) or 2 (liver and spleen). (**E**) Typical H&E stained liver section from an HAV-infected NK cell-depleted *Ifnar1*$^{-/-}$ mouse showing extensive inflammatory infiltrates and hepatocellular apoptosis. NK cell depletion did not alter histopathology. Bar = 50 μm.

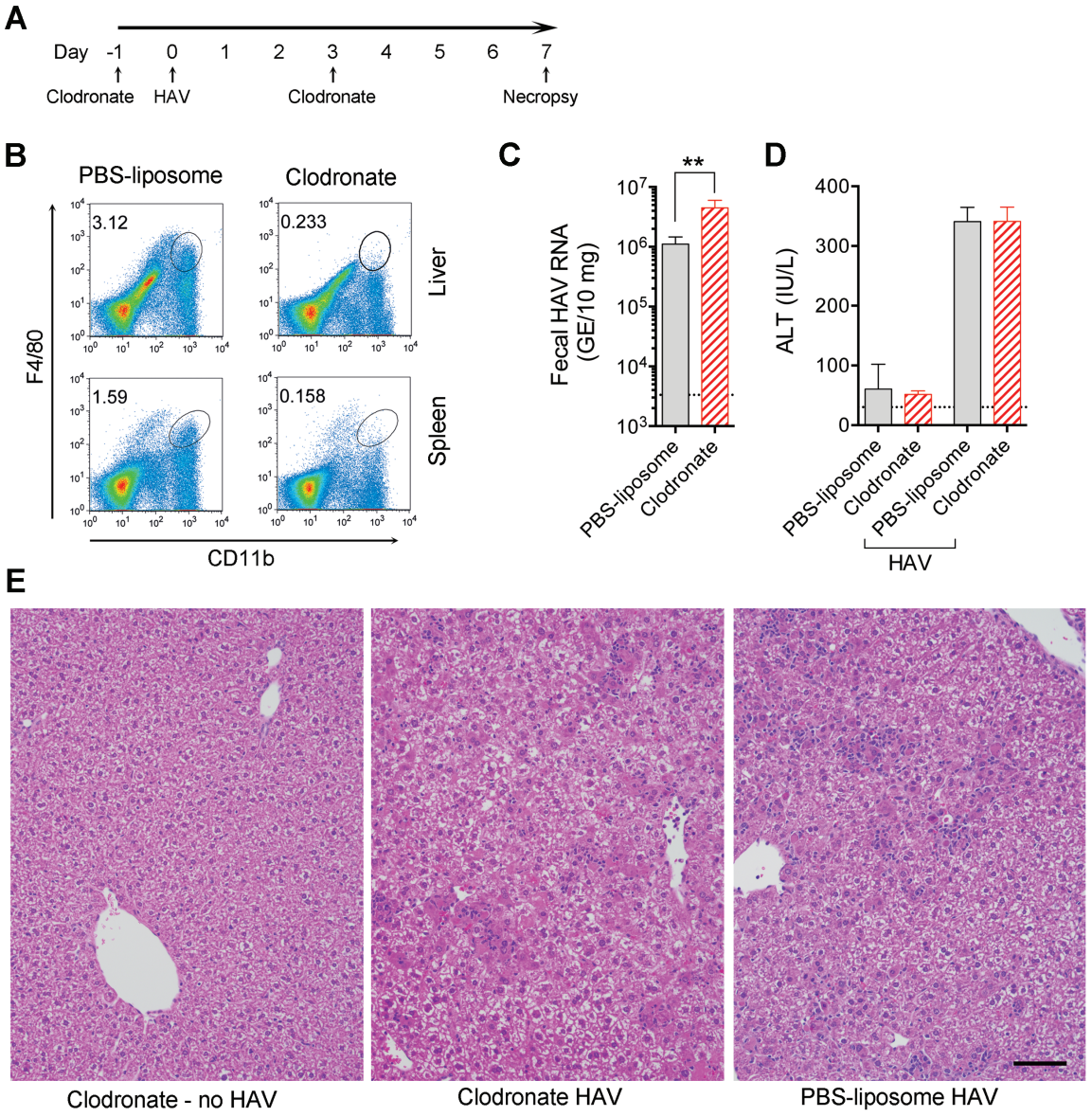


**Fig. S12. HAV infection in macrophage-depleted *Ifnar1*$^{-/-}$ mice.** (**A**) Experimental design: clodronate or control PBS-liposomes were administered i.v. 1 day prior and again 3 days after i.v. HAV challenge. Feces, serum and liver were collected 7 d.p.i. (**B**) Flow cytometry plots of cells from (top) liver and (bottom) spleen of representative HAV-naïve wild-type BL6 mice 24 hrs after i.v. administration of control PBS-liposome or clodronate. Numbers in the upper left quadrant represent the percent F4/80$^{+}$CD11$^{+}$ cells (93% depletion of macrophages from the liver, 90% from spleen). (**C**) Fecal HAV RNA (mean ± SEM) in PBS-liposome versus clodronate liposome treated mice 7 d.p.i., n=7 each; **p=0.007 by two-sided Mann-Whitney test. Horizontal line indicates level of detection. (**D**) Serum ALT (mean ± SEM) in naïve (n=4-5) and HAV-infected PBS-liposome and clodronate liposome treated mice (n=7 each) 7 d.p.i. (**E**) H&E-stained sections of liver from (left) HAV-naïve, clodronate-treated, (center) HAV-infected clodronate-treated, and (right) HAV-infected PBS-liposome treated mice. Bar=50 µm.

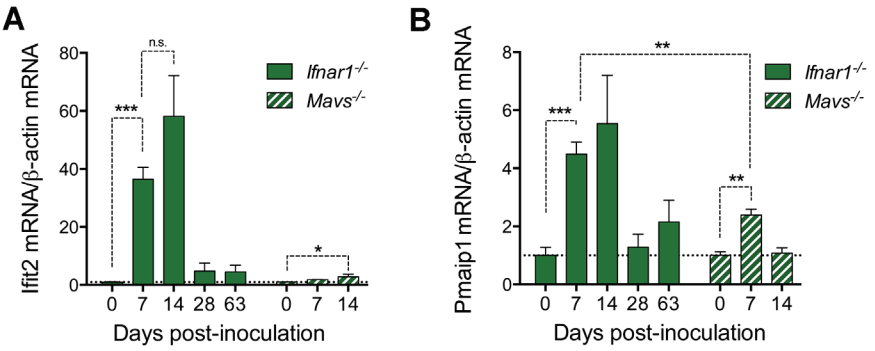


**Fig. S13. *Ifit2* and *Pmaip1* transcriptional responses in HAV-infected *Ifnar1*$^{-/-}$ and *Mavs*$^{-/-}$ mice.** The fold-increase in intrahepatic (**A**) *Ifit2* (ISG54) and (**B**) *Pmaip1* (NOXA) mRNA abundance was determined by RT-qPCR in liver tissue from infected *Ifnar1*$^{-/-}$ (n=4-7) vs. *Mavs*$^{-/-}$ (n=3-7) mice. Data are mean ± SEM, n.s., not significant, *<0.05, **<0.01, ***<0.001 by two-tailed Mann-Whitney test.

**Table S1.** Nonsynonymous changes in HAV polyprotein sequence during passage of virus in DKO mice.

| | Wild-type HM175 GenBank | Chimpanzee Feces 14 d.p.i | Mouse passage 1 Liver 51 d.p.i | Mouse passage 2 Feces 28 d.p.i. | Mouse passage 3 Feces 21 d.p.i. | Mouse passage 4 Liver 18 d.p.i. |
|---|---|---|---|---|---|---|
| Nucleotides sequenced | | 71-7479 | 71-7479 | 71-7415 | 71-7414 | 71-7378 |
| 2C-Glu64 | Glu | Lys | Lys | Lys | Lys | Lys |
| 3D-Ser192 | Ser | Thr | Thr | Thr | Thr | Thr |
| 3D-Arg468 | Arg | - | - | Lys | Lys | Lys |
| GenBank accession | M14707 | KX343014 | KX343015 | KX343016 | KX343017 | KX343018 |

Notes: Near whole-genome sequence was determined by population sequencing of RT-PCR amplimers from virus recovered during the initial 4 passages of HAV in *Ifnar1*$^{-/-}$ *Ifngr1*$^{-/-}$ (DKO) mice (see Fig. 1C). There were no nucleotide changes in the sequenced regions of the 5' and 3' nontranslated RNA segments. "Chimpanzee" virus is the HM175 virus inoculum (chimpanzee fecal extract) (*4*) used for the initial murine challenge. HM175 virus was recovered originally from a naturally-infected human subject in Melbourne, Australia (*45*). '-', no change from wild-type sequence.

**Table S2.** Percent HAV-infected cells, serum ALT and histopathologic findings in representative genetically-deficient mice.

| Genetic knockout | HAV passage | d.p.i. | Mouse # | Liver HAV RNA (GE/ µg RNA) | Percent infected cells (±SEM) | Serum ALT* (IU/L) | Apoptosis/ Inflammation |
|---|---|---|---|---|---|---|---|
| DKO (*Ifnar1*$^{-/-}$*Ifngr1*$^{-/-}$) | 3 | 37 | #2 | $3.3 \times 10^5$ | 8.9 ± 0.9 | 159 | Abundant |
| *Ifnar1*$^{-/-}$ | 5 | 15 | #4 | $3.5 \times 10^6$ | 30.2 ± 7.5 | 373 | Abundant |
| | | | #5 | $4.9 \times 10^6$ | 28.7 ± 4.3 | 358 | Abundant |
| *Mavs*$^{-/-}$ | 5 | 15 | #1 | $2.7 \times 10^7$ | 72.6 ± 5.2 | 36 | Absent |
| | | | #2 | $2.8 \times 10^7$ | 59.6 ± 12 | 20 | Absent |
| *Irf3*$^{-/-}$*Irf7*$^{-/-}$ | 5 | 17 | #11 | $3.3 \times 10^6$ | 11.3 ± 5.3 | 20 | Rare |
| | | | #12 | $6.6 \times 10^6$ | 25.2 ± 11 | 32 | Rare |

*ALT within 2 days of necropsy; upper limits of normal (mean+2 s.d.) = 30.2 IU/L.

Notes: The percent infected cells was estimated by enumerating cells with a positive signal for HAV RNA by *in situ* hybridization versus total nucleated cells in 3-6 representative microscopic fields in each liver (mean total cells counted = 667 ± 58 SEM), as described in Supplementary Materials and Methods. See main text for detailed descriptions of histopathologic findings.

**References**


1. C. Dembek, U. Protzer, Mouse models for therapeutic vaccination against hepatitis B virus. *Med Microbiol Immunol* **204**, 95-102 (2015).
2. B. Y. Winer, Q. Ding, J. Gaska, A. Ploss, In vivo models of hepatitis B and C virus infection. *FEBS Lett*, (2016).
3. R. E. Lanford, S. M. Lemon, C. Walker, in *Hepatitis C Antiviral Drug Discovery & Development,* Y. He, T. Tan, Eds. (Horizons Scientific Press, Norwich, 2011), pp. 99-132.
4. R. E. Lanford, Z. Feng, D. Chavez, B. Guerra, K. M. Brasky, Y. Zhou, D. Yamane, A. S. Perelson, C. M. Walker, S. M. Lemon, Acute hepatitis A virus infection is associated with a limited type I interferon response and persistence of intrahepatic viral RNA. *Proc Nat'l Acad Sci USA* **108**, 11223-11228 (2011).
5. U. Protzer, M. K. Maini, P. A. Knolle, Living in the liver: hepatic infections. *Nat Rev Immunol* **12**, 201-213 (2012).
6. I. N. Crispe, The liver as a lymphoid organ. *Annu Rev Immunol* **27**, 147-163 (2009).
7. J. Kaiser, Biomedical Research: An end to U.S. chimp research. *Science* **350**, 1013 (2015).
8. Z. Feng, L. Hensley, K. L. McKnight, F. Hu, V. Madden, L. Ping, S.-H. Jeong, C. Walker, R. E. Lanford, S. M. Lemon, A pathogenic picornavirus acquires an envelope by hijacking cellular membranes. *Nature* **496**, 367-371 (2013).
9. F. Deinhardt, J. B. Deinhardt, in *Hepatitis A,* R. J. Gerety, Ed. (Academic Press, Inc., Orlando, 1984), pp. 185-204.
10. B. Hornei, R. Kammerer, P. Moubayed, W. Frings, V. Gauss-Muller, A. Dotzauer, Experimental hepatitis A virus infection in guinea pigs. *J Med Virol* **64**, 402-409 (2001).
11. D. A. Feigelstock, P. Thompson, G. G. Kaplan, Growth of hepatitis A virus in a mouse liver cell line. *J Virol* **79**, 2950-2955 (2005).
12. J. F. Drexler, V. M. Corman, A. N. Lukashev, J. M. A. van den Brand, A. Gmyl, S. Brunink, A. Rasche, N. Seggewiss, H. Feng, L. M. Leijten, P. Vallo, T. Kuiken, A. Dotzauer, R. G. Ulrich, S. M. Lemon, C. Drosten, Hepatovirus Ecology Consortium, Evolutionary origins of hepatitis A virus in small mammals. *Proc Nat'l Acad Sci U S A* **112**, 15190-15195 (2015).
13. Y. Yang, Y. Liang, L. Qu, Z. Chen, M. Yi, K. Li, S. M. Lemon, Disruption of innate immunity due to mitochondrial targeting of a picornaviral protease precursor. *Proc Nat'l Acad Sci USA* **104**, 7253-7258 (2007).
14. L. Qu, Z. Feng, D. Yamane, Y. Liang, R. E. Lanford, K. Li, S. M. Lemon, Disruption of TLR3 signaling due to cleavage of TRIF by the hepatitis A virus protease-polymerase processing intermediate, 3CD. *PLoS Pathog* **7**, e1002169 (2011).
15. *Materials and methods are available as supplementary materials at the Science website.*
16. S. M. Lemon, Type A viral hepatitis: new developments in an old disease. *N Engl J Med* **313**, 1059-1067 (1985).
17. J. Pott, T. Mahlakoiv, M. Mordstein, C. U. Duerr, T. Michiels, S. Stockinger, P.

Staeheli, M. W. Hornef, IFN-lambda determines the intestinal epithelial antiviral host defense. *Proc Natl Acad Sci U S A* **108**, 7944-7949 (2011).
18. T. J. Nice, M. T. Baldridge, B. T. McCune, J. M. Norman, H. M. Lazear, M. Artyomov, M. S. Diamond, H. W. Virgin, Interferon-lambda cures persistent murine norovirus infection in the absence of adaptive immunity. *Science* **347**, 269-273 (2015).
19. Y. Lei, C. B. Moore, R. M. Liesman, B. P. O'Connor, D. T. Bergstralh, Z. J. Chen, R. J. Pickles, J. P. Ting, MAVS-mediated apoptosis and its inhibition by viral proteins. *PLoS One* **4**, e5466 (2009).
20. K. Guan, Z. Zheng, T. Song, X. He, C. Xu, Y. Zhang, S. Ma, Y. Wang, Q. Xu, Y. Cao, J. Li, X. Yang, X. Ge, C. Wei, H. Zhong, MAVS regulates apoptotic cell death by decreasing K48-linked ubiquitination of voltage-dependent anion channel 1. *Mol Cell Biol* **33**, 3137-3149 (2013).
21. A. N. Schulman, J. L. Dienstag, D. R. Jackson, J. H. Hoofnagle, R. J. Gerety, R. H. Purcell, L. F. Barker, Hepatitis A antigen particles in liver, bile, and stool of chimpanzees. *J Infect Dis* **134**, 80-84 (1976).
22. C. M. Walker, Z. Feng, S. M. Lemon, Reassessing immune control of hepatitis A virus. *Curr Opin Virol* **11**, 7-13 (2015).
23. H. Ikushima, H. Negishi, T. Taniguchi, The IRF family transcription factors at the interface of innate and adaptive immune responses. *Cold Spring Harb Symp Quant Biol* **78**, 105-116 (2013).
24. H. W. Chen, K. King, J. Tu, M. Sanchez, A. D. Luster, S. Shresta, The roles of IRF-3 and IRF-7 in innate antiviral immunity against dengue virus. *J Immunol* **191**, 4194-4201 (2013).
25. H. M. Lazear, A. Lancaster, C. Wilkins, M. S. Suthar, A. Huang, S. C. Vick, L. Clepper, L. Thackray, M. M. Brassil, H. W. Virgin, J. Nikolich-Zugich, A. V. Moses, M. Gale, Jr., K. Fruh, M. S. Diamond, IRF-3, IRF-5, and IRF-7 coordinately regulate the type I IFN response in myeloid dendritic cells downstream of MAVS signaling. *PLoS Pathog* **9**, e1003118 (2013).
26. S. Faouzi, B. E. Burckhardt, J. C. Hanson, C. B. Campe, L. W. Schrum, R. A. Rippe, J. J. Maher, Anti-Fas induces hepatic chemokines and promotes inflammation by an NF-kappa B-independent, caspase-3-dependent pathway. *J Biol Chem* **276**, 49077-49082 (2001).
27. M. G. Wathelet, C. H. Lin, B. S. Parekh, L. V. Ronco, P. M. Howley, T. Maniatis, Virus infection induces the assembly of coordinately activated transcription factors on the IFN-beta enhancer in vivo. *Mol.Cell* **1**, 507-518 (1998).
28. N. Grandvaux, M. J. Servant, B. tenOever, G. C. Sen, S. Balachandran, G. N. Barber, R. Lin, J. Hiscott, Transcriptional profiling of interferon regulatory factor 3 target genes: direct involvement in the regulation of interferon-stimulated genes. *J Virol* **76**, 5532-5539 (2002).
29. R. Lin, C. Heylbroeck, P. Genin, P. M. Pitha, J. Hiscott, Essential role of interferon regulatory factor 3 in direct activation of RANTES chemokine transcription. *Mol Cell Biol* **19**, 959-966 (1999).
30. B. Rehermann, Natural killer cells in viral hepatitis. *Cell Mol Gastroenterol Hepatol* **1**, 578-588 (2015).
31. F. Marra, F. Tacke, Roles for chemokines in liver disease. *Gastroenterology* **147**,

577-594.e571 (2014).
32. N. C. Reich, A death-promoting role for ISG54/IFIT2. *J Interferon Cytokine Res* **33**, 199-205 (2013).
33. R. Besch, H. Poeck, T. Hohenauer, D. Senft, G. Hacker, C. Berking, V. Hornung, S. Endres, T. Ruzicka, S. Rothenfusser, G. Hartmann, Proapoptotic signaling induced by RIG-I and MDA-5 results in type I interferon-independent apoptosis in human melanoma cells. *J Clin Invest* **119**, 2399-2411 (2009).
34. S. Chattopadhyay, T. Kuzmanovic, Y. Zhang, J. L. Wetzel, G. C. Sen, Ubiquitination of the transcription factor IRF-3 activates RIPA, the apoptotic pathway that protects mice from viral pathogenesis. *Immunity* **44**, 1151-1161 (2016).
35. J. Petrasek, A. Iracheta-Vellve, T. Csak, A. Satishchandran, K. Kodys, E. A. Kurt-Jones, K. A. Fitzgerald, G. Szabo, STING-IRF3 pathway links endoplasmic reticulum stress with hepatocyte apoptosis in early alcoholic liver disease. *Proc Natl Acad Sci U S A* **110**, 16544-16549 (2013).
36. U. Muller, U. Steinhoff, L. F. Reis, S. Hemmi, J. Pavlovic, R. M. Zinkernagel, M. Aguet, Functional role of type I and type II interferons in antiviral defense. *Science* **264**, 1918-1921 (1994).
37. S. Huang, W. Hendriks, A. Althage, S. Hemmi, H. Bluethmann, R. Kamijo, J. Vilcek, R. M. Zinkernagel, M. Aguet, Immune response in mice that lack the interferon-gamma receptor. *Science* **259**, 1742-1745 (1993).
38. N. Althof, S. Harkins, C. C. Kemball, C. T. Flynn, M. Alirezaei, J. L. Whitton, In vivo ablation of type I interferon receptor from cardiomyocytes delays coxsackieviral clearance and accelerates myocardial disease. *J Virol* **88**, 5087-5099 (2014).
39. M. S. Suthar, H. J. Ramos, M. M. Brassil, J. Netland, C. P. Chappell, G. Blahnik, A. McMillan, M. S. Diamond, E. A. Clark, M. J. Bevan, M. Gale, Jr., The RIG-I-like receptor LGP2 controls CD8(+) T cell survival and fitness. *Immunity* **37**, 235-248 (2012).
40. K. Hoebe, X. Du, P. Georgel, E. Janssen, K. Tabeta, S. O. Kim, J. Goode, P. Lin, N. Mann, S. Mudd, K. Crozat, S. Sovath, J. Han, B. Beutler, Identification of Lps2 as a key transducer of MyD88-independent TIR signalling. *Nature* **424**, 743-748 (2003).
41. M. Sato, H. Suemori, N. Hata, M. Asagiri, K. Ogasawara, K. Nakao, T. Nakaya, M. Katsuki, S. Noguchi, N. Tanaka, T. Taniguchi, Distinct and essential roles of transcription factors IRF-3 and IRF-7 in response to viruses for IFN-alpha/beta gene induction. *Immunity* **13**, 539-548 (2000).
42. A. Nakajima, K. Nishimura, Y. Nakaima, T. Oh, S. Noguchi, T. Taniguchi, T. Tamura, Cell type-dependent proapoptotic role of Bcl2L12 revealed by a mutation concomitant with the disruption of the juxtaposed Irf3 gene. *Proc Natl Acad Sci U S A* **106**, 12448-12452 (2009).
43. K. Honda, H. Yanai, H. Negishi, M. Asagiri, M. Sato, T. Mizutani, N. Shimada, Y. Ohba, A. Takaoka, N. Yoshida, T. Taniguchi, IRF-7 is the master regulator of type-I interferon-dependent immune responses. *Nature* **434**, 772-777 (2005).
44. S. Daffis, M. S. Suthar, K. J. Szretter, M. Gale, Jr., M. S. Diamond, Induction of IFN-beta and the innate antiviral response in myeloid cells occurs through an IPS-

1-dependent signal that does not require IRF-3 and IRF-7. *PLoS Pathog* **5**, e1000607 (2009).
45. I. D. Gust, N. I. Lehmann, S. Crowe, M. McCrorie, S. A. Locarnini, C. R. Lucas, The origin of the HM175 strain of hepatitis A virus. *J Infect Dis* **151**, 365-367 (1985).
46. C. Zhao, D. D. Gillette, X. Li, Z. Zhang, H. Wen, Nuclear factor E2-related factor-2 (Nrf2) is required for NLRP3 and AIM2 inflammasome activation. *J Biol Chem* **289**, 17020-17029 (2014).
47. S. M. Lemon, P. C. Murphy, P. A. Shields, L. H. Ping, S. M. Feinstone, T. Cromeans, R. W. Jansen, Antigenic and genetic variation in cytopathic hepatitis A virus variants arising during persistent infection: evidence for genetic recombination. *J Virol* **65**, 2056-2065 (1991).
48. N. A. Counihan, L. M. Daniel, J. Chojnacki, D. A. Anderson, Infrared fluorescent immunofocus assay (IR-FIFA) for the quantitation of non-cytopathic and minimally cytopathic viruses. *J Virol Methods* **133**, 62-69 (2006).
49. M. A. Samuel, J. D. Morrey, M. S. Diamond, Caspase 3-dependent cell death of neurons contributes to the pathogenesis of West Nile virus encephalitis. *J Virol* **81**, 2614-2623 (2007).
50. D. Liu, C. Li, Y. Chen, C. Burnett, X. Y. Liu, S. Downs, R. D. Collins, J. Hawiger, Nuclear import of proinflammatory transcription factors is required for massive liver apoptosis induced by bacterial lipopolysaccharide. *J Biol Chem* **279**, 48434-48442 (2004).
51. Y. Zhou, B. Callendret, D. Xu, K. M. Brasky, Z. Feng, L. L. Hensley, J. Guedj, A. S. Perelson, S. M. Lemon, R. E. Lanford, C. M. Walker, Dominance of the CD4+ T helper cell response during acute resolving hepatitis A virus infection. *J Exp Med* **209**, 1481-1492 (2012).
52. Z. Chen, Y. Benureau, R. Rijnbrand, J. Yi, T. Wang, L. Warter, R. E. Lanford, S. A. Weinman, S. M. Lemon, A. Martin, K. Li, GB virus B disrupts RIG-I signaling by NS3/4A-mediated cleavage of the adaptor protein MAVS. *J Virol* **81**, 964-976 (2007).